# Structural effects of phosphate groups on apatite formation in copolymer modified with $Ca^{2+}$ in a simulated body fluid

Ryo Hamai [1], Hirotaka Maeda [2], Hikaru Sawai [3, 4], Yuki Shirosaki [5],

Toshihiro Kasuga [2], Toshiki Miyazaki [1*]

[1] Graduate School of Life Science and Systems Engineering, Kyushu Institute of Technology, Japan.

[2] Department of Life Science and Applied Chemistry, Nagoya Institute of Technology, Japan.

[3] Fukushima Prefectural Centre for Environmental Creation, Japan.

[4] Institute of Science and Engineering, Kanazawa University, Japan.

[5] Department of Applied Chemistry, Graduate School of Engineering, Kyushu Institute of Technology, Japan.

*Corresponding author:

Toshiki Miyazaki

Graduate School of Life Science and Systems Engineering, Kyushu Institute of Technology, 2-4, Hibikino, Wakamatsu-ku, Kitakyushu, 808-0196, Japan.

Tel/Fax: +81-93-695-6025

E-mail: tmiya@life.kyutech.ac.jp

**Abstract**

Organic-inorganic composites are novel bone substitutes that can ameliorate the mismatch of Young's moduli between natural bone and implanted ceramics. Phosphate groups contribute to the formation of apatite in a simulated body fluid (SBF) and the adhesion of osteoblast-like cells. Therefore, modifications of the polymer with these functional groups are expected to enhance the ability of the organic-inorganic composite to bond with bone. Two phosphate groups have been used, phosphonic acid (-C-$PO_3H_2$) and phosphoric acid (-O-$PO_3H_2$). However, the effects of structural differences between these phosphate groups have not been clarified. In this study, the apatite formation of copolymers modified with $Ca^{2+}$ and either -C-$PO_3H_2$ or -O-$PO_3H_2$ was examined. The mechanism of apatite formation is discussed based on analytical and computational approaches. The copolymers containing -O-$PO_3H_2$, but not those containing -C-$PO_3H_2$, formed apatite in the SBF, although both released similar amounts of $Ca^{2+}$ into the SBF. Adsorption of $HPO_4^{2-}$ from -O-$PO_3H_2$ in the SBF following $Ca^{2+}$ adsorption was confirmed by zeta-potential measurement and X-ray photoelectron spectroscopy. The measurement of the complex formation constant revealed that the -O-$PO_3^{2-}\cdots Ca^{2+}$ complex was thermodynamically unstable enough to convert into $CaHPO_4$, which was not the case

with -C-$PO_3^{2-}\cdots Ca^{2+}$. The formation of $CaHPO_4$-based clusters was found to be a key factor for apatite nucleation. In conclusion, this study revealed that modification with -O-$PO_3H_2$ was more effective for enhancing apatite formation compared with -C-$PO_3H_2$.

**Graphical abstract**

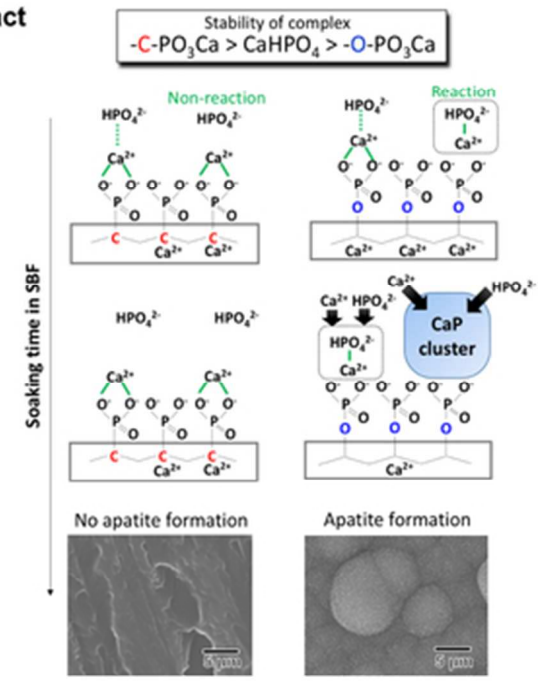


Complex formation of the phosphate on polymers with $Ca^{2+}$ and subsequent reaction with $HPO_4^{2-}$ govern the apatite formation in SBF.

Graphical abstract

43x34mm (300 x 300 DPI)

## 1. Introduction

The ability to bond to existing bone is one of the essential properties for permanent implanted bone substitutes used to repair defects. Bioactive ceramics, such as Bioglass[1], the glass-ceramic A-W[2], and sintered hydroxyapatite[3] can bond to living bone without encapsulation by fibrous tissue. They are able to form bone-like apatite with low levels of crystallinity on their surfaces in physiological environments. Although these materials are used clinically as bone substitutes, implantation may cause stress-shielding and subsequent bone absorption due to their higher Young's moduli compared with natural bone. Natural bone is an organic-inorganic composite consisting of collagen fibers and apatite. Here, the fabrication of artificial bioactive organic-inorganic composites is used to solve this mismatch problem. However, specific functional groups, such as Si-OH [4], Ti-OH [5], carboxyl (-COOH) [6], and sulfonate ($-SO_3H$) [7] can contribute to the formation of a bone-like apatite layer in simulated body fluid (SBF). SBF has inorganic ion concentrations similar to human blood plasma.[8, 9] These groups interact with $Ca^{2+}$ ions in the SBF, and induce heterogeneous nucleation of apatite. Thus, modifications to these functional groups is an important method for preparing composites possessing bone-bonding ability.

Phosphate groups ($-PO_3H_2$) also have attracted a great deal of attention for improving the biocompatibility of implants, and their ability to bond to bone. Tanahashi *et al*. found that phosphate groups immobilized on gold in self-assembled monolayers exhibited better apatite-forming ability compared with carboxyl groups as a result of stronger interactions with $Ca^{2+}$.[6] Datta *et al.* prepared nanofibers and films of poly(vinyl alcohol) modified with phosphate groups via phosphorylation with phosphoric acid.[7] They reported that such modification led to the formation of calcium phosphate in SBF, and the enhancement of the proliferation of osteoblast-like MG63 cells.[10] Moreover, López-Pérez *et al*. showed that the number of SaOs-2 osteoblast-like cells attached on a poly(ε-polycaprolactone) scaffold increased after surface modification using poly(vinylphosphonic acid).[11]

We previously examined the effect of phosphate group content on the apatite-forming ability of copolymers based on vinylphosphonic acid treated with a $CaCl_2$ solution.[12] As a result, an increase in the phosphate group content actually inhibited apatite formation in SBF, despite the fact that the copolymer released $Ca^{2+}$ into the SBF. These results indicate that the incorporation of phosphate groups using vinylphosphonic acid has adverse effect on apatite formation in SBF.

To clarify these different phenomena, we focused on the molecular

structures of the phosphate groups. They have two types of structure, phosphonic acid (-C-$PO_3H_2$) and phosphoric acid (-O-$PO_3H_2$). Tanahashi *et al*. and Datta *et al.* used -O-$PO_3H_2$, while we used -C-$PO_3H_2$. These structural differences are expected to affect the interactions with $Ca^{2+}$ ions, and subsequent apatite formation, because the stability of the ionized phosphate groups is dependent on element substitution as a result of the inductive effect .[13] However, this hypothesis has not previously been examined.

In this study, we prepared copolymers containing $Ca^{2+}$ and either -C-$PO_3H_2$ or -O-$PO_3H_2$ under identical synthetic conditions and examined the apatite formation on their surfaces in SBF. The mechanism of apatite formation on the copolymers is discussed using chemical analytical and computational approaches.

## 2. Materials and methods

### 2.1 Preparation of copolymers modified with $Ca^{2+}$ and different phosphate groups

Vinylphosphonic acid (VPA, 95 %, Tokyo Chemical Industry Co., Ltd., Tokyo,

Japan) and methacryloyloxyethyl phosphate (MOEP, 90%, Phosmer™ M, Yuni

Chemical Co., Ltd., Nara, Japan) were used to incorporate the -C-$PO_3H_2$ and -O-$PO_3H_2$, phosphate groups, respectively, in the copolymers. 2-hydroxyethyl methacrylate (HEMA, 95 %, Wako Pure Chemical Industries, Ltd., Osaka, Japan) and triethylene glycol dimethacrylate (TEGDMA, 90 %, Wako Pure Chemical Industries, Ltd.) were mixed with VPA or MOEP. The molar ratio of the phosphate monomers, HEMA and TEGDMA was VPA:HEMA:TEGDMA = 10:85:5 or MOEP:HEMA:TEGDMA = 7:88:5, and total weight of the monomers was 10 g. Then, 0.5 wt% sodium *p*-toluene sulfinate (*p*-TSS, 98 %, Tokyo Chemical Industry Co., Ltd.) and 2 wt% of *N*,*N*'-dimethyl-*p*-toluidine (97 %, Wako Pure Chemical Industries, Ltd.) were added to the monomers. Then, 1 mol% of (±)-camphorquinone (97 %, Wako Pure Chemical Industries, Ltd.) was added, and the mixture was stirred for 1 hour with light shielding.

Then, the mixture was polymerized for 1 hour using irradiation with blue light (λ=460 nm) and the obtained copolymers were dried at 60°C for 1 day. The copolymers were cut into rectangles and polished with #1000 SiC waterproof abrasive paper. To remove the unreacted regents, the copolymers were soaked in ultra-pure water for one day at room temperature, and dried at 60°C for 1 day. The final size of the copolymers was 10×10×1 mm (weight = 0.1 g). The copolymers

were soaked in 30 $cm^3$ of 0, 0.1, or 1 $kmol \cdot m^{-3}$ $CaCl_2$ solution at 36.5°C for 1 day. The specimens prepared from VPA and MOEP were denoted VPA(C)xCa and MOEP(O)xCa, respectively, and x gives the molarity of the $CaCl_2$ solution used.

**2.2 Soaking specimens in SBF, 1.5CaSBF, or Tris-NaCl buffer**

The SBF ($Na^+$ 142.0, $K^+$ 5.0, $Mg^{2+}$ 1.5, $Ca^{2+}$ 2.5, $Cl^-$ 147.8, $HCO_3^-$ 4.2, $HPO_4^{2-}$ 1.0, $SO_4^{2-}$ 0.5 $mol \cdot m^{-3}$) at pH 7.40 was prepared as follows: NaCl, $NaHCO_3$, KCl, $K_2HPO_4 \cdot 3H_2O$, $MgCl_2 \cdot 6H_2O$, $CaCl_2$, and $Na_2SO_4$ (Nacalai Tesque, Inc., Kyoto, Japan) were dissolved in ultrapure water, and the pH was adjusted with the addition of 1 $kmol \cdot m^{-3}$ HCl and tris(hydroxymethyl) aminomethane (Nacalai Tesque, Inc.). In addition, a solution with a $Ca^{2+}$ concentration 1.5 times that of the final SBF (1.5CaSBF) with a pH 7.25 was also prepared by the same method as the SBF. [14] The specimens were soaked in 30 $cm^3$ of SBF or 1.5CaSBF at 36.5°C for various time intervals.

The Tris-NaCl buffer (NaCl 142, tris(hydroxymethyl) aminomethane 50 $mol \cdot m^{-3}$) at pH 7.40 was prepared by dissolving NaCl and tris(hydroxymethyl) aminomethane in ultrapure water. Then, the pH of the resulting solution was adjusted with the addition of 1 $kmol \cdot m^{-3}$ HCl. The specimens were soaked in 30 $cm^3$ of

Tris-NaCl buffer at 36.5°C for various time intervals to measure the amount of released $Ca^{2+}$.

**2.3 Characterization of the specimens**

To measure the phosphate group content and acid dissociation constant (pKa) of the specimens, 30 $cm^3$ of a 0.16 $kmol \cdot m^{-3}$ NaCl solution, after soaking a VPA(C)0Ca or MOEP(O)0Ca sample in it, was titrated using 0.01 $mol \cdot m^{-3}$ NaOH solution at 36.5°C. During the titration, the pH value of the solution was measured with a pH meter (F-23IIC, Horiba Ltd., Kyoto, Japan).

The Ca content of the specimens before soaking in the SBF was measured by an energy-dispersive X-ray (EDX) analysis system (EMAX Energy, Horiba Ltd.). The surfaces of the specimens after soaking in SBF or 1.5CaSBF were analyzed by thin-film X-ray diffraction (TF-XRD; MXP3V, Mac Science, Co., Yokohama, Japan), X-ray photoelectron spectroscopy (XPS; KRATOS Nova, KRATOS Analytical Ltd., Manchester, UK), and scanning electron microscopy (SEM; S-3500N, Hitachi Co., Tokyo, Japan). For the TF-XRD analysis, the angle of the incident X-rays (CuKα) was fixed at 1° with respect to the surface of the specimens. In the XPS analysis, AlKα ($h\nu$ = 1486.6 eV) was used as the X-ray source, and the

spectra were measured with a high-resolution scan at 20 eV of pass energy. The binding energies of these elemental spectra were calibrated with the binding energy of a methylene group (284.6 eV). The observed spectra was subjected to peak fitting using a blend function consisting of 70% Gaussian and 30% Lorentzian curves.

The zeta-potentials of the surfaces of the specimens were measured with a zeta-potential analyzer (Otsuka Electronics Co., Osaka, Japan) connected to a box-like quartz cell. After being soaked in SBF for various periods, the specimens were washed with ultrapure water, and then placed in the quartz cell. Fresh SBF mixed with polyethylene latex particles (Otsuka Electronics Co.) was introduced into the cell, and the electrophoretic mobilities of the particles were measured using the laser Doppler method to find the zeta-potentials.

The Ca and P concentrations, along with the pH of the SBF and Tris-NaCl buffers after soaking the copolymer specimens with $Ca^{2+}$, were measured with an inductively coupled plasma atomic emission spectrometer (ICP-AES; ICPE-9820, SHIMADZU Co., Kyoto, Japan) and pH meter, respectively.

**2.4 Evaluation of the complex formation constant**

The stability constant of the polymer-$Ca^{2+}$ complex was determined in

accordance with the method reported by Szabadka *et al.*[15] A 0.1 g sample of a VPA(C)0Ca or MOEP(O)0Ca copolymer was soaked in 30 $cm^3$ of a 10 $mol \cdot m^{-3}$ $CaCl_2$ solution for 5 days at 36.5°C. Then, they were soaked in 30 $cm^3$ of the Tris-NaCl buffer, simulating physiological conditions (ion strength: $I$ = 0.16, pH 7.40, 36.5°C), for 5 days. The common logarithm of the stability constant (log β) of the complex in the buffer was calculated using Eqn. (1):

$$\log \beta = \log\left( \frac{[-P_{ion} \cdots Ca^{2+}]}{[*Ca^{2+}][* - P_{ion}]} \right), \quad (1)$$

where $[-P_{ion}\cdots Ca^{2+}]$, $[*Ca^{2+}]$, $[*-P_{ion}]$ are the molar concentrations of the complex of the ionized phosphate groups immobilized in the copolymer, the free calcium ions, and the unbound ionized phosphate groups, respectively, in the Tris-NaCl buffer. These concentration values were calculated using the content of phosphate groups in the copolymer, the pKa of the groups at $I$ = 0.16, and the concentrations of $Ca^{2+}$ in the $CaCl_2$ solution and buffer.

**2.5 Simulation of the dipole moments and molecular orbitals**

The structure with the lowest energy using each of the two phosphate groups was found using the restricted local density approximation and the Perdew-Wang correlational (LDA/PWC) method® with double-numerical basis sets, as

implemented in the DMOl3 software package®.[16, 17] The ground-state geometries were calculated with the phosphate groups bound to Ca as structural models to evaluate their electron density states by the DMOl3. The dipole moments of the species were determined using the Hirshefeld approach.

## 3. Results

Table 1 shows the phosphate group content in the copolymers prepared from different monomers, along with their acid dissociation constants at 36.5°C measured via neutralizing titration. The VPA(C) and MOEP(O) copolymers contained nearly equivalent amounts of the phosphate groups. The first and second proton dissociation constants for MOEP(O) were lower than those of VPA(C).

Figure 1 (A) and (B) show the Ca/P molar ratios of the specimens after treatment with different concentration of the $CaCl_2$ solution, and the Ca concentration in the Tris-NaCl buffer after soaking the specimens. The ratios for the VPA(C) and MOEP(O) samples were very similar with regard to $CaCl_2$ concentration. The Ca concentration in the Tris-NaCl buffer increased and became almost constant after 7 days for all the specimens. The Ca concentrations after 14 days satisfied MOEP(O)1Ca > VPA(C)1Ca ≈ MOEP(O)01Ca > VPA(C)01Ca.

Figure 2 shows the TF-XRD results of the specimens after soaking in SBF for various time intervals. The two broad peaks at 2θ = 26° and 32° corresponding to apatite (JCPDS #09-0432) were observed in MOEP(O)01Ca and MOEP(O)1Ca after 7 days and 1 day, respectively. Conversely, these peaks were not observed in VPA(C)01Ca or VPA(C)1Ca even after 14 days.

Figure 3 shows surface SEM images of different specimens that were soaked in SBF for various time intervals. Deposition was observed on the MOEP(O)01Ca and MOEP(O)1Ca samples after 7 days and 1 day, respectively, but not on the VPA(C)01Ca or VPA(C)1Ca surfaces. The scale-like morphology of the primary particles was similar to the apatite formed in the SBF.[7]

Figure 4(A) shows the XPS spectra of the surfaces of VPA(C)1Ca and MOEP(O)01Ca after soaking in SBF for various time intervals. Peaks attributed to -C-$PO_3H_2$ and -C-$PO_3$Ca were observed in VPA(C)1Ca at 133.2 and 132.7 eV, respectively. [18] The peak position did not shift regardless of the soaking time. In contrast, the peaks attributed to -O-$PO_3H_2$ and -O-$PO_3$Ca were observed in MOEP(O)01Ca at 134.5 and 133.8 eV, respectively.[19] These peaks decreased after 3 hours, while those corresponding to $CaHPO_4$ [20] and octacalcium phosphate (OCP) [21] became visible at 133.4 and 133.2 eV, respectively. Then, the peak corresponding to

apatite was observed at 133.0 eV after 1 day.[22] Figure 4(B) shows the change in the rate for each component of calcium phosphate formed on the MOEP(O)01Ca surface calculated from the area of the fitted peaks in the $P_{2p}$ spectra. The ratio of $CaHPO_4$ to OCP initially increased during the first 3 hours, and then decreased with soaking time. Conversely, the signal from apatite monotonically increased, and the calcium phosphate phase was almost entirely apatite after 7 days.

Figure 5 shows the changes in the surface zeta-potential of the VPA(C)1Ca and MOEP(O)01Ca samples after soaking in the SBF. The potential of both specimens changed from negative to positive after 5 days. Afterwards, the potential of VPA(C)1Ca was almost constant, while that of MOEP(O)01Ca decreased and became negative after 7 days.

Figure 6 shows the changes in the Ca and P concentrations, along with the pH value after soaking the specimens in SBF for various time periods. The Ca concentration after 1 day decreased according to VPA(C)1Ca > MOEP(O)1Ca ≈ MOEP(O)01Ca > VPA(C)01Ca. Then, the Ca concentration gradually decreased in all specimens. The P concentration significantly decreased in MOEP(O)01Ca and MOEP(O)1Ca, while it was almost constant in VPA(C)01Ca and VPA(C)1Ca. The pH value of the SBF following soaking for all the specimens increased after 1 day,

and then gradually decreased.

Figure 7 shows the $P_{2p}$ XPS spectra of the VPA(C)0Ca and MOEP(O)0Ca samples after being soaked in 1.5CaSBF for various time periods. The peaks attributed to -C-$PO_3H_2$ and -C-$PO_3Ca$ were observed in VPA(C)0Ca, and remained constant regardless of the soaking time. On the other hand, the peaks attributed to $CaHPO_4$ and OCP, as well as those from -O-$PO_3H_2$ and -O-$PO_3Ca$, were observed in MOEP(O)0Ca after 3 hours. The peaks from $CaHPO_4$ and OCP were almost replaced by those of apatite after 1 day. This indicates that the initial processes of calcium phosphate formation were similar, irrespective of previous $Ca^{2+}$ incorporation (see Fig. 4).

Table 2 shows the stability constants of the polymer-$Ca^{2+}$ and $CaHPO_4$ (aq.) complex under physiological conditions. The constant for the $CaHPO_4$ (aq.) complex under these conditions was calculated using the ion strength $I$ = 0.02 at 37°C reported by Chughtai e*t al.*[23] The constant increased according to MOEP(O) < $HPO_4^{2-}$ < VPA(C).

Figure 8 shows the structures with the lowest energy from the molecular models of $CH_3$-$CH_2$-$PO_3Ca$ and $CH_3$-$OPO_3Ca$ with -C-$PO_3H_2$ and -O-$PO_3H_2$, respectively. The O atom forms a double bond with P close to the Ca atom in the

$CH_2$-$CH_2$-$PO_3Ca$. On the other hand, this was located in the reverse direction from Ca in $CH_3$-O-$PO_3Ca$. The calculated highest occupied molecular orbital (HOMO) was distributed around the O atoms, while the lowest unoccupied molecular orbital (LUMO) was widely distributed around the Ca atom in both of the phosphate groups. The energy levels of the HOMO and LUMO for $CH_3$-$CH_2$-$PO_3Ca$ were -0.156 and -0.118, and for $CH_3$-O-$PO_3Ca$ they were -0.186 and -0.146 eV, respectively. The value of the dipole moment of $CH_3$-$CH_2$-$PO_3Ca$ was 9.35 Debye, and for $CH_3$-O-$PO_3Ca$ it was 15.71 Debye. This suggests that the structural differences between -C-$PO_3Ca$ and -O-$PO_3Ca$ were not at the molecular orbital level, but rather a result of the most stable structures and polarizability.

**4. Discussion**

Copolymers containing equivalent amounts of the phosphate group and $Ca^{2+}$ were prepared by radical polymerization (See Table 1 and Fig. 1(A)). It was found that the copolymers modified with -O-$PO_3H_2$ had much higher apatite-forming ability in SBF than those modified with -C-$PO_3H_2$ when treated with the $CaCl_2$ solution (See Figs. 2 and 3). This means that modification with -O-$PO_3H_2$ was more effective for apatite formation on the copolymers modified with $Ca^{2+}$, when

compared with -C-$PO_3H_2$.

The formation of embryos, which are pre-nucleation clusters, larger than the critical size *r** are important for the spontaneous nucleation of apatite on the substrate. The activation free energy (ΔG*) for heterogeneous nucleation is given by Eqn. (2) [25]:

$$\Delta G^* = \frac{16\gamma^3 f(\theta)}{3\left(\frac{kT}{V_\beta}\ln(\sigma)\right)^2}, \quad (2)$$

where γ and $V_\beta$, are the interface energies between the nucleus and solution and the molecular volume of the crystalline phase, respectively. On the other hand, $f(\theta)$ is a function of contact angle between the nucleus and the substrate surface, and σ is the supersaturation degree with respect to apatite. σ can be expressed using Eqn. (3):

$$\sigma = \frac{IP_{HAp}}{Ksp_{HAp}}, \quad (3)$$

where $IP_{HAp}$ and $Ksp_{HAp}$ are the ion activity and solubility product with respect to apatite, respectively. Moreover, $IP_{HAp}$ can be calculated from the pH and concentrations of Ca and P using Eqn. (4):

$$IP_{HAp} = (a_{Ca^{2+}})^{10} \cdot (a_{PO_4^{3-}})^6 \cdot (a_{OH^-})^2 \left[Ca^{2+}\right]^{10} \left[PO_4^{3-}\right]^6 \left[OH^-\right]^2, \quad (4)$$

where the values of $a_{Ca^{2+}}$, $a_{PO_4^{3-}}$ and $a_{OH^-}$ are assumed to be 0.36, 0.06, and 0.72 at physiological ionic strength ($I$ = 0.16), respectively, and $Ksp_{HAp}$ is the solubility product for hydroxyapatite ($5.5\times10^{-118}$).[25,26] Therefore, the heterogeneous apatite nucleation in this study was governed by the supersaturation degree and the surface condition of the specimens.

The supersaturation degree with respect to apatite in the SBF can be increased by the release of $Ca^{2+}$ from the substrate [27]. Figure 9 shows the changes in the logarithm of σ in the SBF after soaking the specimens for various time periods. The supersaturation degree decreased as VPA(C)1Ca ≈ MOEP(O)01Ca > VPA(C)01Ca > MOEP(O)1Ca. Although the largest amount of $Ca^{2+}$ was released from MOEP(O)1Ca in the Tris-NaCl buffer (See Fig. 1(B)), the supersaturation degree was low for all specimens. It was speculated that apatite formation on MOEP(O)1Ca occurred rapidly, within 1 day (See Figs. 2 and 3), and that the supersaturation degree rapidly decreased due to ion consumption in the SBF after that time. Although the supersaturation degree values in MOEP(O)01Ca and VPA(C)1Ca were similar, the former formed apatite, but not the latter. These results indicate that structural differences in the phosphate groups affected the surface conditions related to the heterogeneous nucleation of apatite.

It was confirmed by XPS that the surface reaction process was significantly different in -C-$PO_3H_2$ and -O-$PO_3H_2$ (See Fig. 4(A)). VPA(C)1Ca only adsorbs $Ca^{2+}$ to form the -C-$PO_3^{2-}\cdots Ca^{2+}$ complex, but not $HPO_4^{2-}$ in SBF. This is supported by the fact that the P concentration in SBF was almost constant (See Fig. 6). On the other hand, MOEP(O)01Ca formed $CaHPO_4$ and OCP at the initial stage, and subsequently the OCP that formed was transformed into apatite (See Fig. 4(B)). A similar transformation from OCP to apatite on a plasma-treated polymer in SBF was discussed by Oyane *et. al.*[28] These results indicate that only MOEP(O)01Ca adsorbs $HPO_4^{2-}$ following $Ca^{2+}$ adsorption to form calcium phosphate as the precursor of apatite. In addition, MOEP(O)0Ca formed calcium phosphate in 1.5CaSBF even without a release of $Ca^{2+}$ (See Fig. 7). Thus, these results suggest that the specific structures of the phosphate groups provide the surface conditions favorable for apatite nucleation via the adsorption of $HPO_4^{2-}$ in SBF.

It has been reported that the surface zeta-potential is one of the parameters that govern apatite formation on bioactive materials in SBF.[29,30] In the case of titanium metal bound to bone prepared by treatment with an alkaline solution, the negatively charged surfaces becomes positive due to $Ca^{2+}$ adsorption in SBF, then becomes negative again via the subsequent adsorption of phosphate, ultimately

forming apatite.[29] In contrast, VPA(C)1Ca did not demonstrate such behavior, even though the zeta-potential of both specimens changed from negative to positive (See Fig. 5). Based on the results of XPS and the zeta-potential measurement, differences in apatite formation cannot be explained in terms of surface charge alone.

With regard to the initial reaction process for each phosphate group on the surface of specimens with $Ca^{2+}$ and $HPO_4^{2-}$ in the SBF, we consider two viewpoints: (1) the interaction energies between the reactive chemical species in the transition state, and (2) the thermodynamic stability of the products.

With viewpoint (1), it is assumed that a transition state $-PO_3Ca\cdots HPO_4^{2-}$ formed for all the specimens. The interaction energy is obtained as the sum of the frontier orbital interaction and the Coulomb interaction.[31, 32] The LUMO around the Ca atom in the both model (See Fig. 8) was expected to accept the HOMO electron of $HPO_4^{2-}$. When comparing the energy levels of the orbitals, a significant difference is observed for the LUMO in both models (-0.146 and -0.118 eV) and the HOMO level of O atoms in $HPO_4^{2-}$ (-8.9 eV) estimated from the vertical ionization energy.[33] This means that the Coulomb interaction contributes more to the formation of the transition state than the frontier orbital. A computational simulation of the polarizability indicated that the Coulomb interaction of the $-O-PO_3^{2-}\cdots Ca^{2+}$ complex

with $HPO_4^{2-}$ was stronger than with -C-$PO_3^{2-}\cdots Ca^{2+}$. Therefore, the transition state in MOEP(O) was predicted to be more stable than VPA(C), leading to a decrease in activation energy for the formation of $CaHPO_4$ in the former.

Using viewpoint (2), the thermodynamic stability values between $CaHPO_4$ (aq.) and the complex composed of $Ca^{2+}$ and one of the phosphate groups were evaluated. The magnitude of the complex formation constants in Table 2 indicate that $Ca^{2+}$ bound with MOEP(O) has a higher ability to bond to $HPO_4^{2-}$ via a ion-dipole interaction, and subsequently become converted into $CaHPO_4$, because the stability of the -O-$PO_3^{2-}\cdots Ca^{2+}$ complex was lowest.

The $Ca^{2+}\cdots HPO_4^{2-}$ interaction on the surface of the MOEP(O) sample had an important role for apatite deposition. It was recently reported that heterogeneous apatite nucleation on a titanium substrate treated with $H_2O_2$ in SBF progresses via the formation of a pre-embryo consisting of $Ca^{2+}$, $HPO_4^{2-}$, and $OH^-$.[34, 35] Moreover, self-assembled monolayers containing carboxyl groups formed clusters by accumulation of pre-nucleation complexes of $[Ca(HPO_4)_3]^{4-}$.[36, 37]

Summarizing the mechanism described above, apatite formation on the surface of MOEP(O) is assumed to progress as follows: an increase in $[Ca(HPO_4)_3]^{4-}$ concentration results in the formation of many clusters larger than $r^*$. Subsequently,

the clusters transformed to OCP, the apatite precursor, via ion adsorption in the SBF. In fact, Habraken *et al.* demonstrated that amorphous calcium phosphate with the formula $[Ca_2(HPO_4)_3]^{2-}$ grew into Ca-deficient OCP via the aggregation of the pre-nucleation complex and ions in a solution supersaturated with respect to the apatite.[37]

Finally, the results of this study reveal that differences in the molecular structures of the phosphate groups govern the apatite-forming ability of the copolymers modified with $Ca^{2+}$, because the low thermodynamic stability of the phosphate$\cdots Ca^{2+}$ complex on the specimen enhances calcium phosphate cluster formation that is favorable for apatite nucleation. It is also expected that such structural differences affect the ability of the composites to bond with bone. Recently, Huang *et al.* reported that modification of -O-$PO_3H_2$ promoted the differentiation of mesenchymal stem cells to provide the mineralization on the polymer.[38] However, it has been nerve reveled whether structural difference affects behavior of calcification induced by the cells. To clarify this point in detail, the adsorption behavior of protein, and the response the cells, should be investigated in future work.

## 5. Conclusion

The structural effects of phosphate groups on apatite formation on the surface of copolymer modified with $Ca^{2+}$ in SBF were examined. The copolymers modified with phosphoric acid (-O-$PO_3H_2$) induced heterogeneous nucleation of apatite, but not those modified with phosphonic acid (-C-$PO_3H_2$), because the amount of adsorbed $HPO_4^{2-}$ in the SBF was insufficient for apatite nucleation. The reason for this phenomenon was that the thermodynamic stability of the ionized -O-$PO_3^{2-}\cdots Ca^{2+}$ complex was lower than -O-$PO_3^{2-}\cdots Ca^{2+}$. It was found that the reaction with $HPO_4^{2-}$ that allowed the calcium phosphate clusters to become precursors of apatite was a key issue that significantly affected apatite formation on the copolymer.

**Acknowledgments**

This study was supported by Grant-in-Aid for JSPS Research Fellow Grant Number 17J02000. We thank Louis R. Nemzer, Ph.D., from Edanz Group (www.edanzediting.com/ac) for editing a draft of this manuscript.

**Reference**

1. L. L Hench, *J. Am. Ceram. Soc.*, 1998, **81**, 1707-1728.

2. T. Kokubo, H.M. Kim, M. Kawashita, *Biomatrials*, 2003, **24**, 2161-2175.

3. M. Jarcho, C. H. Bolen, M. B. Thomas, J. Bobick, J. F. Kay, R. H. Doremus, *J. Mater. Sci*., 1976, **11**, 2161-2175.

4. S. B. Cho, K. Nakanishi, T. Kokubo, N. Soga, T. Kamamura, T. Kitsugi, T. Yamamuro, *J. Am. Ceram. Soc.*, 1995, **78**, 1769-1774.

5. M. Uchida, H.M. Kim, T. Fujibayashi, T. Nakamura, *J. Biomed. Mater. Res. A*, 2003, **64**, 164-170.

6. M. Tanahashi, T. Matsuda, *J. Biomed. Mater. Res.*, 1997, **34**, 305-315.

7. T. Kawai, C. Ohtsuki, M. Kamitakahara, T. Miyazaki, M. Tanihara, Y. Sakaguchi, S. Konagaya, *Biomaterials*, 2004, **25**, 4529-4534.

8. S. B. Cho, K. Nakanishi, T. Kokubo, N. Soga, C. Ohtsuki, T. Nakamura, T. Kitsugi, T. Yamamuro, *J. Am. Ceram. Soc*., 1995, **78**, 1769-1774.

9. T. Kokubo, H. Takadama, *Biomaterials*, 2006, **27**, 2907-2915.

10. P. Datta, J. Chatterjee, S. Dhara, *Collids Surf. B Biointerfaces*, 2012, **94**, 177-183.

11. P. M. López-Pérez, R. M. P. Silva, R. A. Sousa, I. Pashkuleva, R. L. Reis, *Acta Biomater*. 2010, **6**, 3704-3712.

12. R. Hamai, Y. Shirosaki, T. Miyazaki, *J. Mater. Sci.: Mater. Med*., 2016, **27**,

152.

13. O. Exner, *J. Phys. Org. Chem.*, 1999, **12**, 265-274.

14. S. B. Cho, F. Miyazi, T. Kokubo, K. Nakanishi, N. Soga, T. Nakamura, *J. Ceram. Soc. Japan*, 1996, **104**, 399-404.

15. Ö Szabadka, E. Varga, L. Nagy, *Talanta*, 2003, **59**, 1081-1088.

16. J. P. Perdew, Y. Wang, Accurate and simple analytic representation of the electron gad correlation energy, *Phys. Rev. B*, 1992, **45** 13244-13249.

17. B. Delly, From molecules to solids with the DMOl3 approach, *J. Chem. Phys.*, 2000 **113**, 7756-7764.

18. X. Zhou, S. H. Goh, S. Y. Lee. *Polymer*, 1997, **38**, 5333-5338.

19. I. F. Amaral, P. L. Granja, M. A. Barbosa, *J. Biomater. Sci. Polym. Ed.*, 2005, **16**, 1575-1593.

20. T. Hanawa, M. Ota, *Biomaterials*, 1991, **12,** 767-774.

21. M. J. Van Stiodonk, D. R. Justes, E. A. Schweikert, *Anal. Chem.*, 1999, **71**, 149-153.

22. L. Radev, M. H. V. Fernandes, I. M. Salvado, D. Kovacheva, *Cent. Eur. J. Chem.*, 2009, **7**, 721-730.

23. A. Chughtai, R. Marshall, G. H. Nancollas, *J. Phys. Chem.*, 1968, **72**, 208-211.

24. T. Kawai, C. Ohtsuki, M. Kamitakahara, M. Tanihara, T. Miyazaki, Y. Sakaguchi, S. Konagaya, *J. Ceram. Soc. Japan*, 2005, **113**, 588-592.

25. W. Neuman, M. Neuman, *University of Chicago, Chicago,* 1958, 3-3.

26. H. McDowell, T. M. Gregory, W. E. Brown, *J. Res. Nat. Bur. Stand. A. Phys. Chem.*, 1977, **81**, 273-281.

27. C. Ohtsuki, T. Kokubo, T. Yamamuro, *J. Non-Cryst. Soilds*, 1992, **43**, 84-92.

28. A. Oyane, M. Uchida, Y. Yokogawa, C. Choong, J. Triffitt, A. Ito, *J. Biomed. Mater Res. A*., 2005, **75**,138-145.

29. H.-M. Kim, T. Himeno, M. Kawashita, J.-H. Lee, T. Kokubo, T. Nakamura, *J. Biomed. Mater. Res. A*., 2003, **67**, 1305-1309.

30. H.-M. Kim, T. Himeno, T. Kokubo, T. Nakamura, *Biomaterials*, 2005, **21**, 4366-4373.

31. *Chemical Reactivity and Reaction Path*s ed. G. Klopman, Wiley-Interscience New York, 1974.

32. G. Klopman. *J. Am. Chem. Soc.*, 1968, **90**, 223-234.

33. E. Pluhařová, M. Ončák, R. Seidel, C. Schroeder, W. Schroeder, B. Winter, S. E. Bradforth, P. Jungwirth, P. Slavíček, *J. Phys. Chem. B*, 2012, **116**, 13254-13264.

34. S. Hayakawa, K. Tsuru, K. Uetsuki, K. Akasaka, Y. Shirosaki, A. Osaka, *J.*

*Mater. Sci: Mater. Med.*, 2015, **26**, 222.

35. K. Uetsuki, S. Nakai, Y. Shirosaki, S. Hayakawa, A. Osaka, *J. Biomed. Mater. Res. A*, 2013, **101**, 712-719.

36. A. Dey P. H. H. Bomans, F. A. Müller, J. Will, P. M. Frederik, G. With, N. A. J. M. Sommerdijk, *Nat. Mater.*, 2010, **9**, 1010-1014.

37. W. J. E. M. Habraken, J. Tao, L. J. Brylka, H. Friedrich, L. Bertinetti, A. S. Schenk, A. Verch, V. Dmitrovic, P. H. H. Bomans, P. M. Frederik, J. Laven, P. Schoot, B. Aichmayer, G. With, J. J. DeYoreo, N. A. J. M. Sommerdijk, *Nat. Commun.*, 2013, **4**, 1507.

38. P. Huang, X. Bi, J. Gao, L. Sun, S. Wang, S. Chen, X. Fan, Z. You, Y. Wang, *J. Mater. Chem. B.*, 2016, **4**, 2090-2101.

**Table 1** Phosphate group content (n = 3) and acid dissociate constant at 36.5℃ of different copolymer measured by neutralizing titration

| | VPA(C) | MOEP(O) |
|---|---|---|
| Phosphate group / mmol・$g^{-1}$ | 0.24±0.02 | 0.24±0.002 |
| $pKa_1$ | 3.63 | 3.48 |
| $pKa_2$ | 6.11 | 5.96 |

**Table 2** Stability constants of ionized phosphate group-$Ca^{2+}$ complex on the different polymers (n = 4) in comparison with that of $CaHPO_4$ complex under the physiological condition.

| | VPA(C) | $CaHPO_4$(aq.) | MOEP(O) |
|---|---|---|---|
| log β | 4.44±0.07 | 3.41 | 3.08±0.13 |

**Figure captions**

**Figure 1** Ca/P molar ratio of the specimens after soaking in 0.1 or 1 kmol·m$^{-3}$ of $CaCl_2$ solution (A) and Ca concentration in Tris-NaCl buffer following soaking of the different specimens (n = 3) (B).

**Figure 2** TF-XRD patterns of the specimens following soaking in SBF for various periods.

**Figure 3** SEM images of the surfaces of the specimens following soaking in SBF for various periods.

**Figure 4** $P_{2p}$ XPS spectra of VPA(C)1Ca and MOEP(O)01Ca (A) and change in rate of component of calcium phosphate formed on the MOEP(O)01Ca (B) following soaking in SBF for various periods.

**Figure 5** Change in surface zeta potential of VPA(C)1Ca and MOEP(O)01Ca following soaking in SBF for various periods (n = 3).

**Figure 6** Change in Ca and P concentrations and pH in SBF following soaking of different specimens (n = 3).

**Figure 7** $P_{2p}$ XPS spectra of VPA(C)0Ca and MOEP(O)0Ca following soaking in 1.5CaSBF for various periods.

**Figure 8** The structure of molecular model of (A) $CH_3$-$CH_2$-$PO_3Ca$ and (B)

$CH_3$-O-$PO_3$Ca with the lowest energy for each type of phosphate groups (white: H, gray: C, red: O, purple: P, green: Ca atom).

**Figure 9** Change in supersaturation degree with respect to the apatite in SBF following soaking of different specimens (n = 3).

**Figure 1**

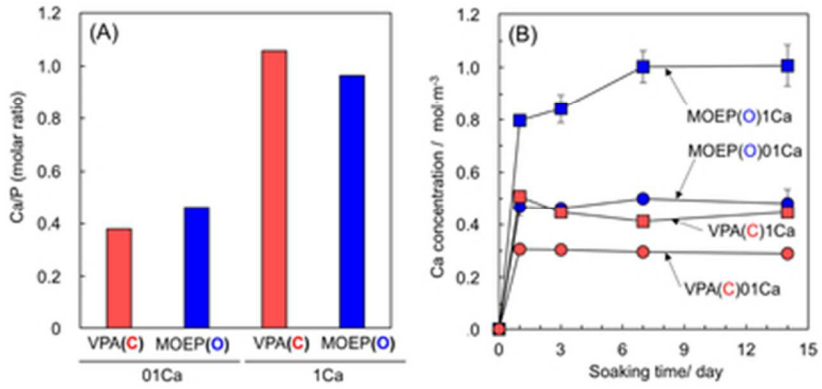


Fig.1

36x22mm (300 x 300 DPI)

**Figure 2**

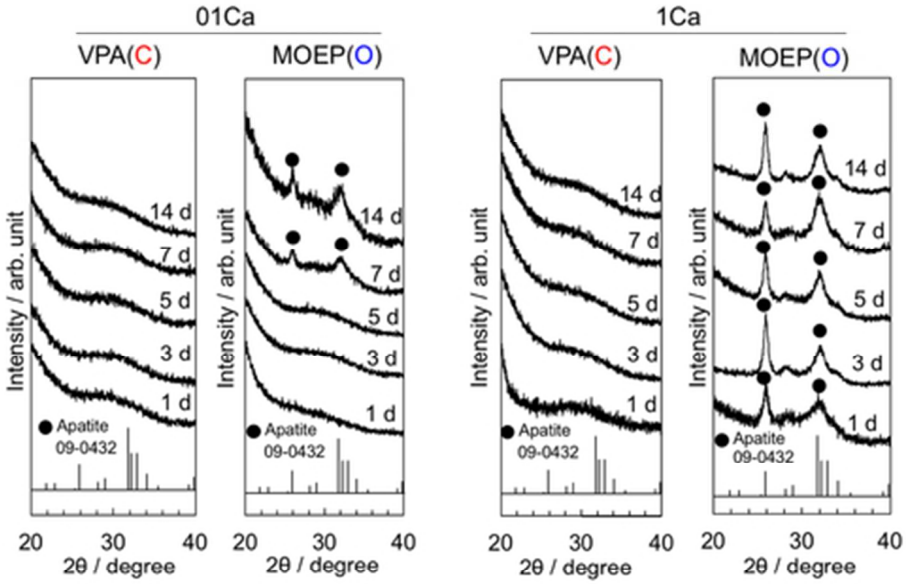


Fig.2

44x33mm (300 x 300 DPI)

**Figure 3**

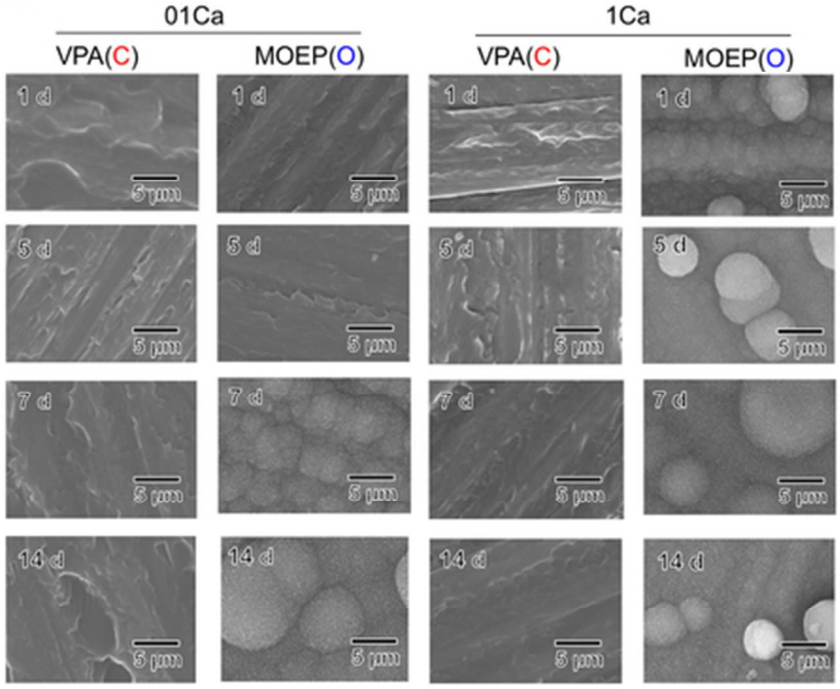


Fig.3

44x33mm (300 x 300 DPI)

**Figure 4(A)**

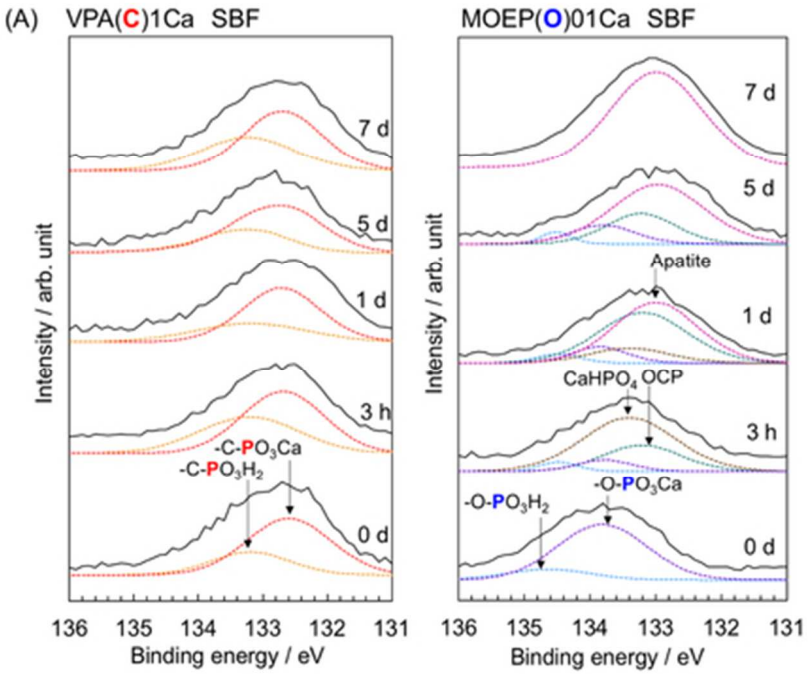


Fig.4A

44x33mm (300 x 300 DPI)

**Figure 4(B)**

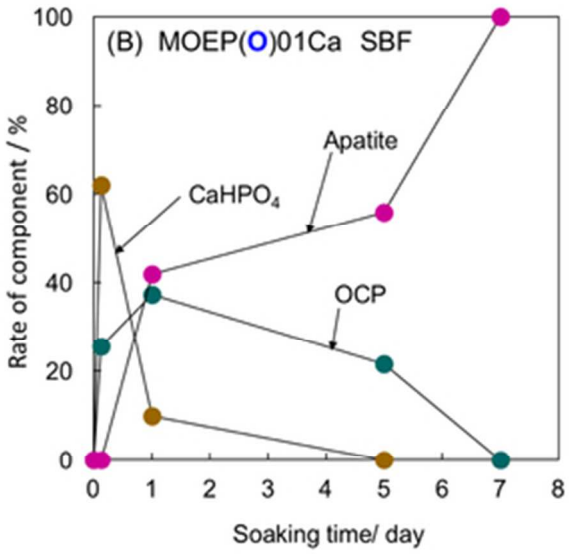


Fig.4B

38x29mm (300 x 300 DPI)

**Figure 5**

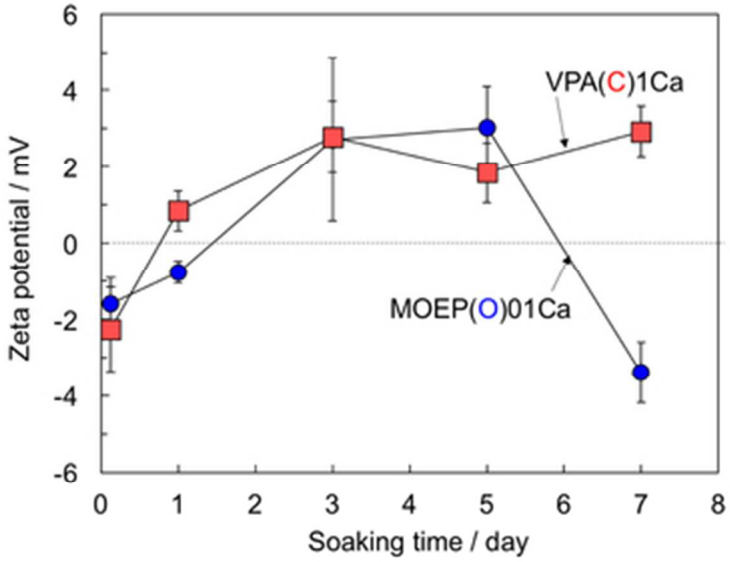


Fig.5

41x31mm (300 x 300 DPI)

**Figure 6**

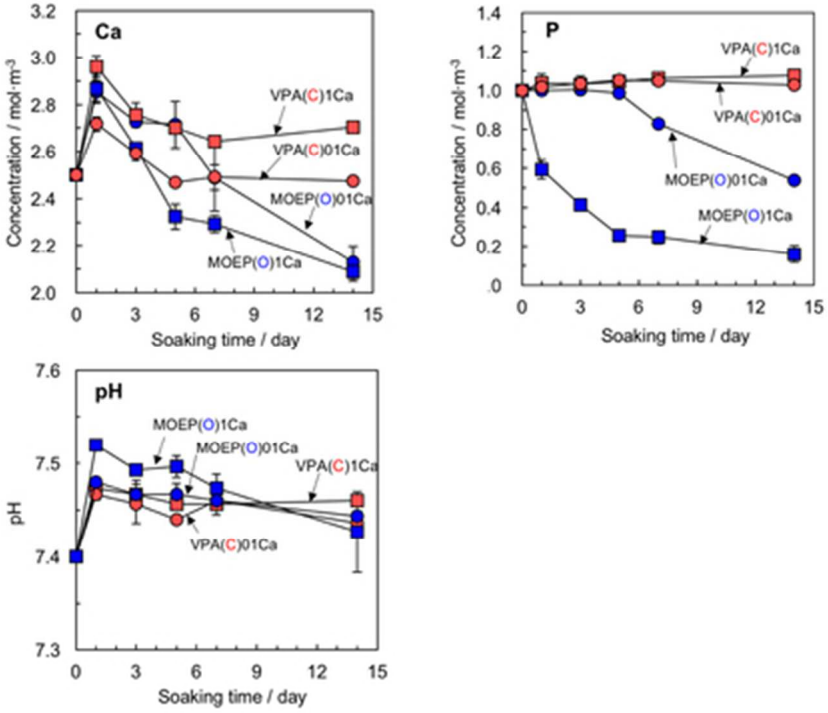


Fig.6

42x32mm (300 x 300 DPI)

**Figure 7**

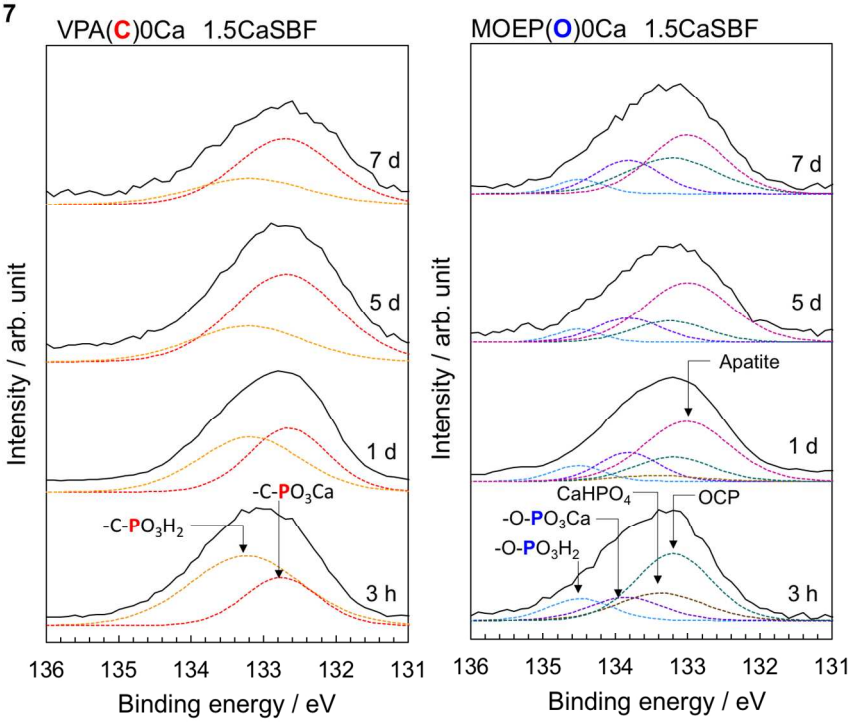


Fig.7

254x190mm (160 x 160 DPI)

Figure 8

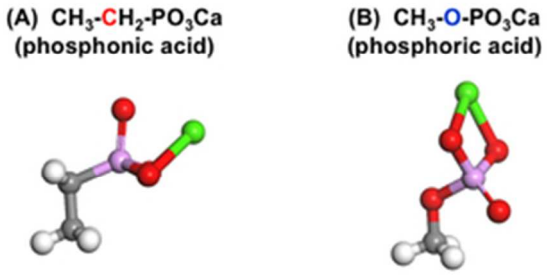


Fig.8

26x15mm (300 x 300 DPI)

**Figure 9**

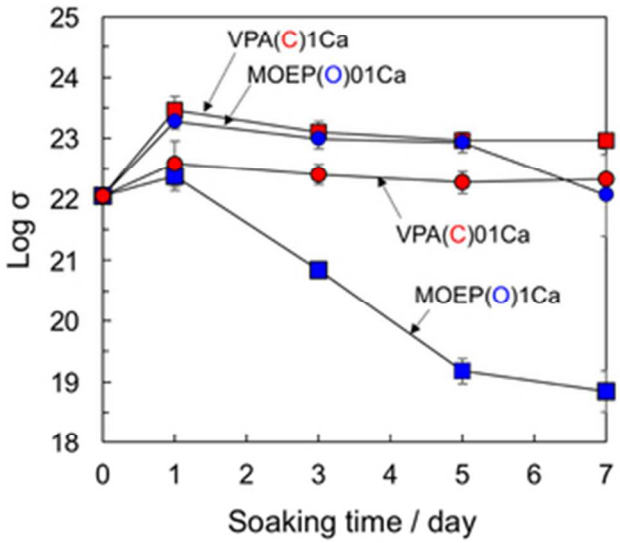


Fig.9

33x28mm (300 x 300 DPI)